Analysis of a Three-Phase Flying Converter Cell Rectifier Operating in Light/No-Load Condition

M. Makoschitz*, M. Hartmann† and H. Ertl*
* Institute of Energy Systems and Electrical Drives, Power Electronics Section
University of Technology Vienna, Austria; Email: markus.makoschitz@tuwien.ac.at

† Schneider Electric Power Drives, Section Drives, Power Conversion
Vienna, Austria; Email: michael.hartmann@ieee.org

***Abstract*—The "Flying" Converter Cell (FCC) rectifier allows the extension of an existing passive diode bridge rectifier to a low-harmonic unity power factor input stage by adding a combination of additional converter topologies to the DC-side of the passive circuit. In general, light-load condition of such an active rectifier, however, may lead to undesired effects as, e.g., impaired total harmonic distortion of input currents ($\mathrm{THD_i}$). In this paper the operation of the active rectifier circuit under no-load or light-load conditions and corresponding effects are therefore analyzed in detail also considering the control of the two FCC DC voltages. Three different operating modes are proposed and different parameters and characteristics of these modes are discussed accompanied by simulation results. It is shown that the inductance value of the coupled three-phase current injection choke directly influences the operating behavior and design guidelines for this coupled inductor are therefore derived. This work further comprises a closer look at current control and voltage balancing of FCC DC voltages during light- and no-load condition and resulting optimization issues evoked due to appropriate control of dedicate control structures. Discussed side effects are finally verified by experimental results taken from a laboratory prototype of 10 kW output power and 10 kHz switching frequency.**

***Index Terms*—Three-Phase AC-DC Conversion, Third-Harmonic Injection, No-Load Operation**

I. Introduction

Active three-phase PFC rectifier systems are widely used in industry if high (unity) power factor and low harmonic input currents are required. Topologies as, e.g., the six-switch boost-type PFC rectifier (bidirectional power flow) [1], [2], Vienna Rectifier (unidirectional power flow) [3], six-switch buck-type PFC rectifier (unidirectional power flow, for positive dc output voltage), SWISS Rectifier (unidirectional power flow) [4] or the "hybrid third harmonic current injection active-filter rectifier" (unidirectional power flow) [1], [5] are perfectly suitable to full-fill the IEEE519/IEC61000-3-2 standards [6], [7] for mitigation of input current harmonics. Major drawbacks of these rectifier ciruits are that (at least) two active semiconductor components have to process the full amount of output power and none of these structures can be used to extend an existing passive three-phase rectifier to a low harmonic input stage.

A hybrid system ([8]) based on the third harmonic injection principle has therefore been introduced ([9]) which allows the extension of an existing passive three-phase diode bridge rectifier to a low-harmonic current input stage by adding an additional converter stage - known as "Flying" Converter Cell (FCC) active rectifier (see **Fig. 1**) - to the DC-side of the passive circuit. The active system only needs to process some small

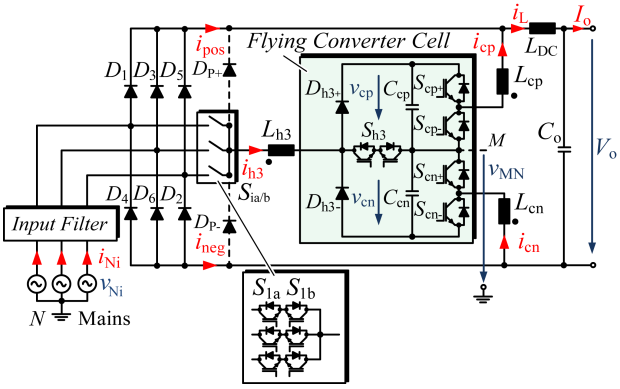

Fig. 1: Simplified schematic of an active rectifier circuit employing a "Flying" converter cell as proposed in [9].

amount of the rated output power and therefore shows improved efficiency, unity power factor ($\lambda > 0.99$) and low harmonic input currents ($\mathrm{THD_i} < 5\%$) (cf., [10]). The FCC basically consists of three different converter topologies (two half-bridges and one unidirectional three-level bridge leg). Both half-bridges have to inject such amount of current i_{cp} and i_{cn} into the positive and negative busbar (primarily formed by the output of the passive diode bridge rectifier) to guarantee sinusoidal waveshapes i_{pos} and i_{neg}. The unidirectional three-level bridge leg is cyclically connected to the AC-side mains and injects a third harmonic current i_{h3}. The system only allows uncontrolled DC output voltage V_{o} which is defined by the mains voltages $V_{\mathrm{o}} = \frac{3\sqrt{3}\hat{V}_{\mathrm{N}}}{\pi}$ during continuous conduction mode operation and no common-mode voltage components v_{CM} with switching frequency f_{s} appear.

Passive three-phase diode bridge rectifier circuits on the other hand are a favourable solution for low-cost applications which require high efficiency ($\eta_{\mathrm{B6}} \approx 99\%$) and increased input current distortion and reduced power factor are admissible. Due to the low circuit complexity of the system side effects during light and no-load mode (as for example increased output voltage) can be easily adressed and investigated. The described modes are very well known in literature, namely "continuous conduction mode" (CCM) and "discontinuous conduction mode" (DCM). DCM, however, has to be seperated into two different modes - $\mathrm{DCM_I}$ and $\mathrm{DCM_{II}}$ ([11]). The term CCM is typically referring to the state of the rectifiers inductor current i_{L}. Considering the passive three-phase rectifier, CCM is applicable if the DC-

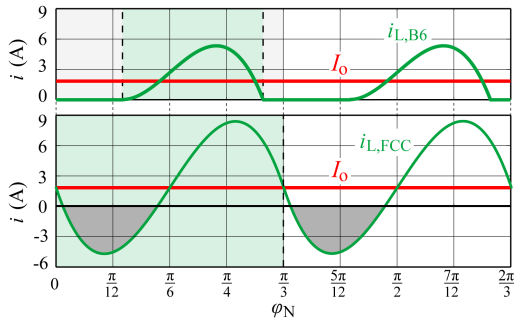

Fig. 2: Numerically and analytically calculated DC-side smoothing inductor current regarding passive $i_{L,B6}$ (DCM_{II}) and active rectification $i_{L,FCC}$, respectively, for a rated output power of approximately 1 kW and a DC-side smoothing choke value of 2.25 mH for a 10 kW rectifier system.

side smoothing inductor current is of positive value during a whole period $[0 \ldots 2\pi]$. The so called "discontinuous conduction mode" typically shows at least one section where the current of the DC inductor equals 0 A. For both CCM and DCM no high frequency common-mode voltage can be observed and the maximum output voltage is given due to its physical limitations defined by the mains voltages ($V_{o,max} = \sqrt{3}\hat{V}_N$).

As briefly discussed in [10] this discontinuous state based on the DC-side smoothing inductance current never occurs for the hybrid system due to the active FCC topology which is able to process positive and negative current values, also depicted in **Fig. 2**. The passive rectifier system shows increased output voltage ($V_o \approx 550$ V instead of 537.5 V) for an output power of approximately 1 kW and is operating in DCM_{II} mode, whereas the active system still operates in continuous conduction mode (CCM) for the same load ($L_c = 2$ mH) and hence an output voltage V_o of the expected 537.5 V can be observed. The peak-to-peak 300 Hz DC-side choke current component is, however, considerably higher for FCC operation than for passive rectification which results in increased inductor losses for light loads of the active system and therefore reduced efficiency η_{FCC}.

The discontinuous mode for the hybrid system is rather related to the current situation of the positive and negative busbar currents i_{pos} and i_{neg}. As these currents are not assigned to any choke, the state is not designated as "discontinuous conduction mode" but rather denominated as "intermittent current operating mode" (ICOM). The FCC can be operated in different modes during ICOM which basically depends on the behaviour of the bidirectional switch arrangement connected to the AC-side of the passive system. This paper consideres three different modes which are defined as specific "operating mode" (OM). Three different operating modes are therefore defined by

- **Operating Mode I** (OM_I): FCC fully in operation, however, current injection devices ($S_1 - S_3$) disabled
- **Operating Mode II** (OM_{II}): FCC fully in operation including current injection devices
- **Operating Mode III** (OM_{III}): FCC operation stopped (only passive diode bridge operating)

Benefits and drawbacks of the appropriate modes are discussed in the following, wher symmetric values of the coupled three-phase injection choke $L_{cp} = L_{cn} = L_{h3} = L_c$ and perfectly balanced FCC DC voltages $v_{cp} = v_{cn} = V_c$ are assumed.

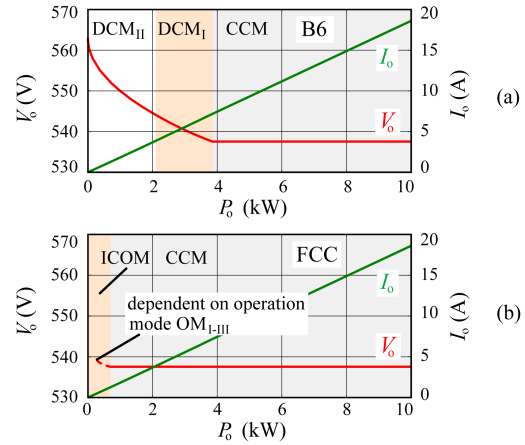

Fig. 3: Calculated output characteristics V_o and I_o for an output power range from no-load operation (0 W) to nominal load (10 kW) considering (a) CCM, DCM_I and DCM_{II} of a passive three-phase diode bridge rectifier (upper figure) with $L_{DC} = 2.25$ mH and (b) CCM and ICOM of the hybrid rectifier utilizing a FCC (lower graph) for an injection inductance L_c of 2 mH.

II. Continuous to Discontiuous Operation Boundaries

Before investigating the differnt operating modes (OM_{I-III}) for intermittent currents i_{pos} and i_{neg} of the hybrid system in detail, an elaborate analyzes for both, passive system CCM to DCM boundary (i_L) and active system CCM to ICOM (intermittent current operating mode) boundary (i_{pos},i_{neg}) has to be determined. The DC-side smoothing inductance current i_L for continuous conduction mode is therefore required which calculates to

$$i_{L,CCM}(\varphi_N) = I_o - \frac{3\sqrt{3}\hat{V}_N}{\pi\omega_N L_{DC}} \sum_{k=1}^{\infty} \frac{2}{(6k)^3 - 6k} \sin(6k\varphi_N) \quad (1)$$

with $k = 1, 2, \ldots$, where I_o is the output current of the system and ω_N the angular frequency. **Eq. (1)** is valid for both, the passive and the active system while operating in CCM. The threshold between CCM and DCM of the passive system can therefore be found at $i_{L,CCM}(\varphi_N) = 0$ A which yields an appropriate output power level of

$$P_{o,CCM/DCM_I} = \frac{3(3\hat{V}_N)^2}{\pi\omega_N L_{DC}} \left(\frac{1}{\pi} \arcsin\left(\frac{3}{\pi}\right) - \frac{1}{2} + \ldots \right. \\ \left. \ldots + \frac{1}{\pi}\sqrt{\left(\frac{\pi}{3}\right)^2 - 1} \right). \quad (2)$$

If a passive system for a rated output power of 10 kW and a DC-side smoothing inductance of 2.25 mH for an appropriate THD_i of $\approx 48\,\%$ is assumed the CCM to DCM_I threshold computes to $P_{o,CCM/DCM_I}(L_{DC} = 2.25\text{mH}) \approx 4$ kW. Starting from this reference point, the output voltage cannot longer be considered to be $V_{o,max} = \frac{3\sqrt{3}\hat{V}_N}{\pi} = 537.5$ V but is increasing for decreasing loads and limited to $V_{o,max} = \sqrt{3}\hat{V}_N = 563$ V. The averaged output voltage can be calculated numerically for discontinuous conduction mode and is plotted in **Fig. 3(a)**.

As announced in section I the transition from CCM to ICOM for the FCC topology originates from the current situation of the

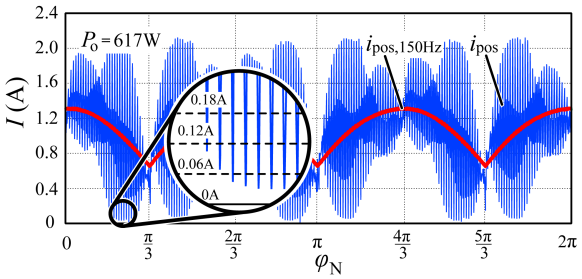

Fig. 4: Simulated current i_{pos} for the calculated output power regarding CCM/ICOM boundary. A three-phase injection inductance L_{c} of 2 mH, DC-side smoothing inductance L_{DC} of 2.25 mH, a switching frequency f_{s} of 10 kHz and FCC DC voltages V_{c} of 400 V are assumed.

positive and negative busbar currents of the passive diode bridge rectifier. Considering ideal current waveforms neglecting the switching frequency ripple, 0 A sections regarding i_{pos} and i_{neg} can only be found for $P_{\mathrm{o}} = 0\,\mathrm{W}$. This leads to the assumption that the CCM to ICOM boundary does not only depend on the low frequency current component of i_{pos} and i_{neg} but is also dependent on the high switching frequency ripple evoked due to the coupled three-phase injection inductance L_{c} and its design. In order to calculate the mentioned state threshold, the minimum of the positive busbar current $\min\left(i_{\mathrm{pos,CCM}}\right)$ for CCM light-load conditions needs to be evaluated, which can be found at $\varphi_{\mathrm{N}} \approx \pi/3$. The transition from CCM to ICOM is available if one half of the maximum ripple (at $\pi/3$) equals (or appears to be larger than) the averaged sinusoidal waveshape i_{pos} during this time instant which can be stated by the following equation

$$\frac{\Delta i_{\mathrm{cp,pkpk}}}{2} = \hat{I}_{\mathrm{N}} \cdot \cos\left(\frac{\pi}{3}\right). \tag{3}$$

An appropriate power level can hence be assessed by

$$P_{\mathrm{o,CCM/ICOM}} = \frac{M V_{\mathrm{c}}^2 \left(\frac{3}{4}M - \frac{1}{2\sqrt{3}}\right)\left(1 - \frac{\sqrt{3}}{2}M\right)}{f_{\mathrm{s}} L_{\mathrm{c}}} \tag{4}$$

using the coupled three-phase inductance guidlines derived in [9]. The CCM to ICOM threshold (cf., **Fig. 3(b)**) therefore yields

$$P_{\mathrm{o,CCM/ICOM}}\Big|_{V_{\mathrm{c}}=400\,\mathrm{V},\ L_{\mathrm{c}}=2\,\mathrm{mH},\ f_{\mathrm{s}}=10\,\mathrm{kHz}} \approx 600\,\mathrm{W}. \tag{5}$$

In **Fig. 4** simulation results of the FCC topology for the given constraints are depicted. Comparing **eq. (2)** and **eq. (4)** the CCM to DCM boundary of the passive system shows inverse proportional behaviour of the DC-side smoothing inductance L_{DC}, whereas the boundary between contionous to intermittent currents i_{pos} and i_{neg} of the hybrid system is independent of L_{DC} but yields $1/x$-dependency of the coupled three-phase inductor L_{c}.

The active system can hence operate in CCM for a wide power range if the injection inductance is appropriatly designed which mainly results in a very good input current quality for the respective load region.

III. FCC Operation During No/Light-Load Condition

In contrast to the passive rectifier which could not yield negative inductor current values ($i_{\mathrm{L,B6}} \geq 0$, cf., **Fig. 2**) due

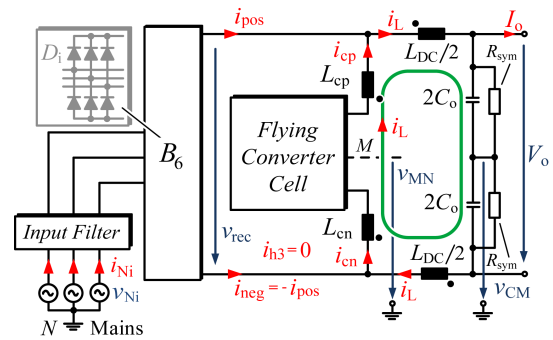

Fig. 5: Basic schematic of active rectifier topology during no-load condition while operating in $\mathrm{OM_I}$. Circulating current i_{L} (green) leads to unfavourable additional losses during no- and light-load mode.

to its semiconductor arrangement (passive diode bridge), the inductor current ($i_{\mathrm{L,FCC}}$) of the FCC system never shows zero current gaps during light/no-load condition (**Fig. 2**). This is caused by the FCC topology which is able to provide positive and negative current values, as already discussed in section I. While the diode bridge is blocking for negative current fractions of i_{pos} and i_{neg}, i_{L} occurs as **circulating current** which has to be processed by the FCC, the DC-side smoothing inductor L_{DC} and the DC-link voltage capacitor C_{o} during no-load condition. This circular current causes additional losses compared to a passive system during no-load operation (inductor losses L_{DC} and L_{c}, switching and conduction losses etc.) and shows a high frequency current ripple with switching frequency.

A. Operating Mode I ($\mathrm{OM_I}$)

In $\mathrm{OM_I}$ (**Fig. 5**) the current injection device ($S_1 - S_3$) is disabled during no-load operation and the third harmonic injection current i_{h3} therefore equals zero. This leads to identical busbar current values ($|i_{\mathrm{pos}}| = |i_{\mathrm{neg}}|$) while the diodes are conducting, which can be also verified by

$$\begin{aligned} i_{\mathrm{h3}} = i_{\mathrm{cp}} - i_{\mathrm{cn}} = 0 \implies i_{\mathrm{cp}} &= i_{\mathrm{cn}} \\ i_{\mathrm{pos}} &= i_{\mathrm{L}} - i_{\mathrm{cp}} \\ i_{\mathrm{neg}} &= i_{\mathrm{cn}} - i_{\mathrm{L}} \\ \implies i_{\mathrm{pos}} &= -i_{\mathrm{neg}}\,. \end{aligned} \tag{6}$$

Only four different switching states of the FCC therefore occur during no-load mode ($S_{\mathrm{cp+}} = 0$ and $S_{\mathrm{cn+}} = 0$; $S_{\mathrm{cp+}} = 1$ and $S_{\mathrm{cn+}} = 0$; $S_{\mathrm{cp+}} = 0$ and $S_{\mathrm{cn+}} = 1$; $S_{\mathrm{cp+}} = 1$ and $S_{\mathrm{cn+}} = 1$, 1...corresponding switch closed). The passive diode bridge is blocking each time $S_{\mathrm{cp+}} = 1$ and $S_{\mathrm{cn+}} = 0$ is valid, as the maximum FCC DC voltage $2V_{\mathrm{c}} > \sqrt{3}\hat{V}_{\mathrm{N}}$ applies. In section $\varphi_{\mathrm{N}} \in \left[0 \ldots \frac{\pi}{6}\right]$, power flow ($i_{\mathrm{pos}} = i_{\mathrm{neg}} = 0$) from the grid to the DC-side is not possible if $v_{\mathrm{N1}} - v_{\mathrm{N3}} < v_{\mathrm{rec}}$ is valid, which means that the passive rectifier diodes are stressed with a high frequency component with switching frequency f_{s}.

As the bidirectional switches are not operated anymore, the averaged midpoint voltage of the FCC ($v_{\mathrm{MN,avg}}$) cannot longer be controlled to zero. The different voltage levels of the FCC midpoint voltage v_{MN} are therefore characterized by an additional low frequency 150 Hz voltage component which is given due to the mains voltage situation and further depending on the half-bridge switching states which now yield 0 V, v_{Ni},

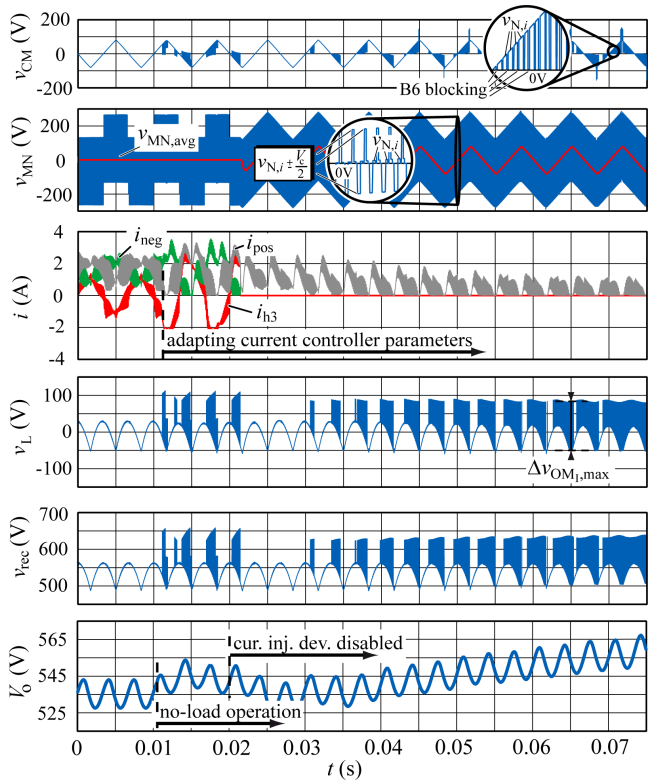

Fig. 6: Simulation results considering notable parameters as common-mode output voltage v_{CM}, midpoint to neutral point voltage v_{MN}, DC-side currents i_{pos}, i_{neg}, i_{h3}, rectifier output voltage v_{rec}, DC-side smoothing inductance voltage v_{L} and output voltage of the active rectifier syste V_{o}, for continuous conduction mode and no-load mode ($\mathrm{OM_I}$).

$v_{\mathrm{Ni}} \pm V_{\mathrm{c}}/2$ instead of 0 V, $\pm 2V_{\mathrm{c}}/3$, $\pm V_{\mathrm{c}}/3$ for the appropriate FCC control described in [10].

The low frequency common-mode voltage v_{CM} is defined by the mains voltage situation (e.g. $v_{\mathrm{CM}} = v_{\mathrm{N2}}/2$ for $\varphi_{\mathrm{N}} \in \left[0 \ldots \frac{\pi}{6}\right]$) during conduction of the passive rectifier diodes and is zero while the passive diode bridge is blocking (due to increased DC-side voltage levels). As can be observed from **Fig. 6**, v_{CM} is therefore characterized by a voltage ripple with switching frequency in this mode.

If the diode bridge is not conducting the DC-side choke L_{DC} is stressed by an increased voltage defined due to the DC-side voltage situation which addresses additional high frequent (f_{s}) losses for the DC-side smoothing inductance during no-load mode. Due to the circulating current for no-load mode the inductor losses are defined by

$$P_{L_{\mathrm{DC}}} = P_{\mathrm{Cu,DC}} + P_{\mathrm{Cu,AC}}\left(6 \cdot f_{\mathrm{N}}, f_{\mathrm{s}}\right) + P_{\mathrm{Fe}}\left(6 \cdot f_{\mathrm{N}}, f_{\mathrm{s}}\right) \quad (7)$$

The maximum applied peak-to-peak voltage $\Delta v_{\mathrm{OM_I,max}}$ as depicted in **Fig. 6** is defined by

$$\Delta v_{\mathrm{OM_I,max}} = \frac{L_{\mathrm{DC}}}{L_{\mathrm{c}} + L_{\mathrm{DC}}/2} \frac{V_{\mathrm{c}}}{2} \,. \quad (8)$$

The FCC rectifier system furthermore shows an increase of the output voltage V_{o} during no-load operation. As the limit for a conventional passive rectifier system is defined by the mains maximum line-to-line voltage level

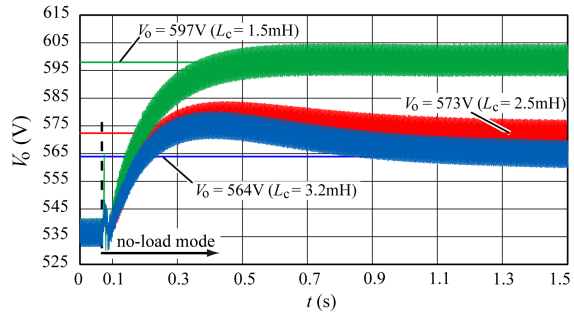

Fig. 7: Simulation results of the active rectifier system ($\mathrm{OM_I}$) regarding output voltage V_{o} for different injection inductance values L_{c} and appropriate calculated values (coloured horizontal lines).

($V_{\mathrm{o,max}} = V_{\mathrm{ij,max}} = \sqrt{3}\hat{V}_{\mathrm{N}} = 563\,\mathrm{V}$), the maximum output voltage of the active system is characterized by the inductance value of the coupled three-phase inductor L_{c} and calculates to

$$\Delta V_{\mathrm{o,idle}} = V_{\mathrm{c}} \frac{\left(\frac{3\sqrt{3}}{\pi}M - 1\right)\frac{L_{\mathrm{DC}}}{L_{\mathrm{c}}+L_{\mathrm{DC}}/2}\left(1 - \frac{3\sqrt{3}}{2\pi}M\right)}{1 - \frac{L_{\mathrm{DC}}}{L_{\mathrm{c}}+L_{\mathrm{DC}}/2}\left(1 - \frac{3\sqrt{3}}{2\pi}M\right)} \quad (9)$$

where M denotes the modulation index and is given by $\hat{V}_{\mathrm{N}}/V_{\mathrm{c}}$ (hence $M = \sqrt{2} \cdot 230\,\mathrm{V_{eff}}/400\,\mathrm{V} = 0.813$). **Fig. 7** illustrates simulation results considering the output voltage V_{o} of the active rectifier system while operating in no-load mode for different inductance values L_{c}. As previously described, increased output voltages can be observed and the steady state output voltage levels are in good agreement with the calculated output voltages using **eq. 9**. The appearing time constant of the load step characteristic (V_{o} response in **Fig. 7**) is caused by the physical and digital implementation of hardware and software of the passive system and the active FCC.

In conclusion, during operation of $\mathrm{OM_I}$ and no-load condition, (i) an increased output voltage V_{o}, (ii) additional losses due to circulating current i_{L} with superimposed high frequency current ripple and (iii) a high frequency common-mode voltage v_{CM} have to be expected.

B. Operating Mode II ($\mathrm{OM_{II}}$)

As already mentioned in secion I the three different modes $\mathrm{OM_{I-III}}$ are defined by the operating state of the FCC during ICOM. $\mathrm{OM_{II}}$ is valid if ICOM is detected by the system and all bidirectional switches connected to the AC-side of the hybrid system are still operated. In contrast to the control method for the Vienna Rectifier proposed in [12], where the switches are controlled differently for CCM and DCM, the six switches attached to the FCC active rectifier still continue pursuing their 90° low switching duty each phase while operated in $\mathrm{OM_{II}}$. Consequently, the FCC is still cyclically connected to the AC-side mains even for no-load mode operation.

The passive three-phase rectifier can be considered as two M_3-structures with diodes (D_1, D_3, D_5) and forward biased during the positive half-waves and the negative midpoint structure $M_{3,\mathrm{neg}}$ whose diodes (D_2, D_4, D_6) are forward biased during the negative half-waves. It is essential to distinguish between these two diode assemblies, as in contrast to CCM, $\mathrm{OM_I}$ or $\mathrm{OM_{III}}$, both M_3-structures are not only conducting at

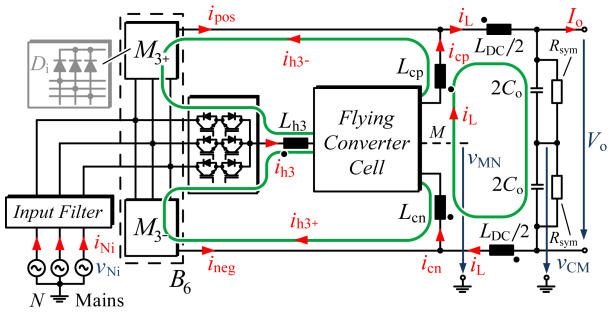

Fig. 8: Schematic of FCC active rectifier operating in $\mathrm{OM_{II}}$ during no-load condition. As bidirectional switch topology still active, two different circulating currents occur (i_{h3} and i_{L}), causing increased losses compared to $\mathrm{OM_I}$.

the same time for $\mathrm{OM_{II}}$ but also conducting seperately, which is primarily evoked due to the operating three-level unidirectional bridge leg (S_{h3}, $D_{\mathrm{h3}\pm}$). Considering ideally controlled currents i_{pos} and i_{neg}, $i_{\mathrm{h3,150Hz}}$ can be assumed to equal zero as the electrictal conductance value $g_{\mathrm{e}}^{*} = 0$ (cf., [10] - current control of FCC). The three-level bridge, however, still generates a high frequency current ripple with switching frequency $\Delta i_{\mathrm{h3},f_{\mathrm{s}}}$, which can be compared with no-load characteristics of half- or three-level bridge legs. This continuous current ripple, however, has to be processed by an alternative circuit path during no-load mode which has to be provided by one of the midpoint structures $M_{3,\mathrm{pos}}$ or $M_{3,\mathrm{neg}}$ (depeding on the sign of the third harmonic injection current). The diode assembly is hence offering an alterative current path, depending on the AC- and DC-side voltage situation and the sign of the generated current i_{h3}, very similar to a "Freewheeling" diode of a e.g. buck converter topology. The remaining midpoint structure is blocking and therefore not conducting any current. This high frequent current ripple hence appears as circulating current (cf., **Fig. 8**). $\mathrm{OM_{II}}$ hence causes two differing circiulating currents i_{L} and i_{h3}. In order to validate the discussed issues a third harmonic injection current ripple $i_{\mathrm{h3},f_{\mathrm{s}}} < 0\,\mathrm{A}$ is assumed. As previously mentioned, the negative midpoint structure $M_{3,\mathrm{neg}}$ is blocking which leads to $i_{\mathrm{neg}} = 0$ and i_{cn} therefore can be computed to

$$\begin{aligned} i_{\mathrm{cn}} &= i_{\mathrm{neg}} + i_{\mathrm{L}} \\ \Longrightarrow\ i_{\mathrm{cn}} &= i_{\mathrm{L}}\ . \end{aligned} \tag{10}$$

The positive busbar current i_{pos} can therefore be calculated to $i_{\mathrm{pos}} = -i_{\mathrm{h3}}$. The current i_{pos} hence equals negative injection current i_{h3} if $M_{3,\mathrm{neg}}$ is blocking. Similarly, the same assumptions made for $i_{\mathrm{h3},f_{\mathrm{s}}} > 0\,\mathrm{A}$ lead to $i_{\mathrm{cp}} = i_{\mathrm{L}}$ and hence $i_{\mathrm{neg}} = -i_{\mathrm{h3}}$. As the injection inductance (L_{h3}) potential is still defined by the AC-side mains (due to operating bidirectional switches), the midpoint voltage $v_{\mathrm{MN,avg}}$ can still be controlled to be zero which is also depicted in **Fig. 9**.

Similar to $\mathrm{OM_I}$, the DC-side smoothing inductance L_{DC} shows increased (high frequent (f_{s})) losses during no-load mode while operating in $\mathrm{OM_{II}}$ which is basically evoked due to alternating blocking of the two midpoint structures (further resulting in a high frequency common-mode voltage v_{CM} with switching frequency f_{s} shown in **Fig. 9**). An increased peak-to-peak voltage v_{L} can therefore be observed. The maximum voltage $\Delta v_{\mathrm{OM_{II},max}}$ across the DC-side choke can be calculated

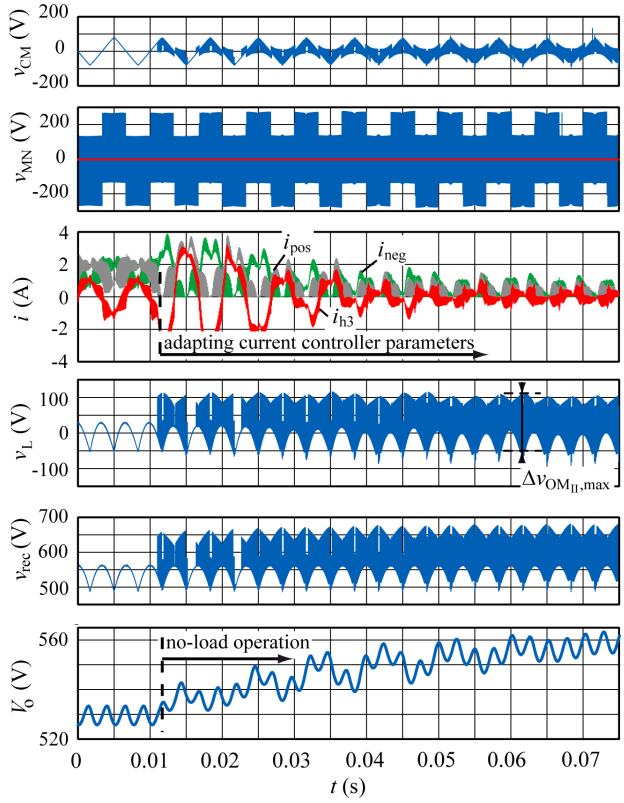

Fig. 9: Simulation results considering notable parameters as common-mode output voltage v_{CM}, midpoint to neutral point voltage v_{MN}, DC-side currents i_{pos}, i_{neg}, i_{h3}, rectifier output voltage v_{rec}, DC-side smoothing inductance voltage v_{L} and output voltage of the active rectifier syste V_{o}, for continuous conduction mode and no-load mode ($\mathrm{OM_{II}}$).

to

$$\Delta v_{\mathrm{OM_{II},max}} = \frac{L_{\mathrm{DC}}}{L_{\mathrm{c}} + L_{\mathrm{DC}}/2}\frac{3V_{\mathrm{c}}}{5} \tag{11}$$

As can be noticed, the maximum applied peak-to-peak voltage $\Delta v_{\mathrm{OM_{II},max}}$ is approximately 20 % larger for $\mathrm{OM_{II}}$ than for $\mathrm{OM_I}$ ($\Delta v_{\mathrm{OM_{II},max}} = 1.2 \cdot \Delta v_{\mathrm{OM_I,max}}$).

Both operating modes furthermore show increased output voltages. The final output voltage V_{o} is defined by the inductance ratio between L_{c} and L_{DC} similarly as for $\mathrm{OM_I}$. The output voltage level, however, appears to be much higher as only one duty cycle δ_{cp} or δ_{cn} is mandatory, primarily depending on which midpoint structure is blocking. The output voltage $V_{\mathrm{o,idle}}$ can hence be computed to

$$\Delta V_{\mathrm{o,idle}} = V_{\mathrm{c}}\frac{\frac{3\sqrt{3}}{2\pi}M\frac{L_{\mathrm{DC}}}{L_{\mathrm{c}}+L_{\mathrm{DC}}/2}\left(1-\frac{3\sqrt{3}}{2\pi}M\right)}{1-\frac{1}{2}\frac{L_{\mathrm{DC}}}{L_{\mathrm{c}}+L_{\mathrm{DC}}/2}\left(1-\frac{3\sqrt{3}}{2\pi}M\right)}\ . \tag{12}$$

Fig. 10 shows simulated and calculated steady state output voltage values for different injection inductance values L_{c}.

C. Operating Mode III ($\mathrm{OM_{III}}$)

For operating mode III, the FCC circuitry is completely switched off (only the passive diode bridge is operating) which means that the system shows discontinuous mode behavior very

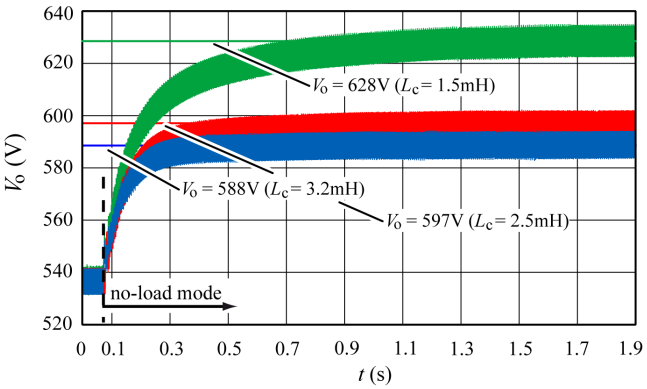

Fig. 10: Simulation results of the active rectifier system regarding output voltage V_o while operating in OM_{II} for different injection inductance values L_c and appropriate calculated values (coloured horizontal lines) which obviously results in divergent output voltage levels.

well known for a passive diode bridge rectifier. Depending on the ICOM boundary, the active system directly enters DCM_I or DCM_{II} when getting disabled. The difference between those two discontinuous operation modes is defined by the input or DC-side smoothing inductance current characteristic as depicted in **Fig. 11**. The rectifier output voltage v_{rec} and the DC-side inductance current i_L consist of four different sectors (I-IV) for DCM_I. Considering DCM_{II} only two different sectors can be found anymore, which is defined due to the increased 0 A current gap and the hence missing commutation process of the passive diode bridge. The boundary between these two discontinuous modes is characterized by $i_L\left(\varphi_N = \gamma = k\frac{\pi}{3}\right) = 0\text{A}$ for $k \in \mathbb{Z}$ which leads to a specific output power value $P_{o,DCM12}$

$$P_{o,DCM_{I/II}} = \frac{3\sqrt{3}\hat{V}_N V_o}{\pi\omega_N L_{DC}}\left(\frac{V_o}{\sqrt{3}\hat{V}_N} - \frac{\sqrt{3}}{2} + \ldots\right.$$
$$\ldots + \left(\frac{\pi}{3} - \alpha_D\right)\sqrt{1 - \frac{1}{3}\left(\frac{V_o}{\hat{V}_N}\right)^2}\Bigg) + \ldots \tag{13}$$
$$\ldots + \frac{3V_o^2}{\pi\omega_N L_{DC}}\left(\left(\frac{\pi}{3} - \alpha_D\right)\alpha_D - \frac{\left(\frac{\pi}{3}\right)^2 - \alpha_D^2}{2}\right)$$

which can be approximately calculated to 1.9 kW for a given DC-side smoothing inductor value of 2.25 mH, negligence of output voltage ripple ($C_o \rightarrow \infty$) and $\alpha_D = -\frac{\pi}{3} + \arcsin\left(\frac{V_o}{\sqrt{3}\hat{V}_N}\right)$. It has to be mentioned that $V_o = \frac{3\sqrt{3}\hat{V}_N}{\pi}$ is no longer valid for discontinuous conduction mode and has to be evaluated numerically. Exactly like OM_I and OM_{II}, also OM_{III} leads to increased output voltage levels of V_o during discontinuous mode. The output voltage, however, is limited due to the mains situation to $V_{o,idle,max} = \sqrt{3}\hat{V}_N$.

As the FCC is completely disabled, no high frequency common-mode voltage at the output of the system appears. Only the typical low frequency 150 Hz component can be observed which is slightly differing in its characteristic (compared to the conduction mode waveform) due to the blocking passive diode bridge instants. For no-load operation the ideal passive diode bridge does not show any currents or circulating currents and is therefore loss-free, which is not valid for OM_I and OM_{II} as

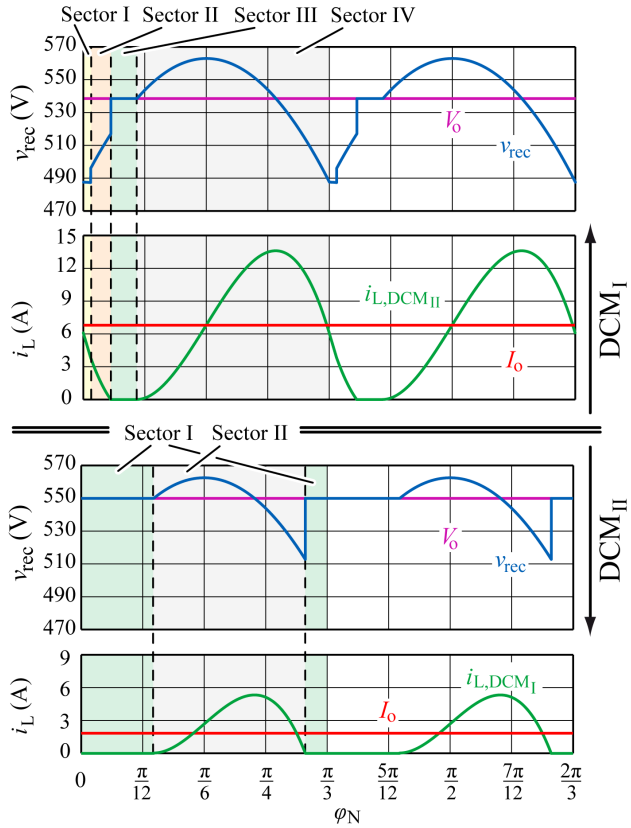

Fig. 11: Calculated passive three-phase rectifier bridge voltage v_{rec}, system output voltage V_o and DC-side smoothing inductance current i_L for discontinuous conduction mode I and II of a passive system (FCC deactivated - OM_{III}). Depending on the designed injection inductance L_c, the system enters DCM_I or DCM_{II} during light-load mode if the active topology going to be deactivated.

discussed in previous sections.

IV. Enhanced Design Guidlines

In the following some guidance to select the inductance value of the three-phase choke L_c is given considering also limitations of operation in light/no-load condition. As mentioned before both operating modes (OM_I and OM_{II}) show a high dependency on the designed three-phase inductance value L_c. The maximum inductance value of the coupled three-phase choke L_c is usually defined by the maximum ripple current. A specific amount of voltage V_c, however, is required for proper current shaping which limits the inductance L_c for a given FCC DC voltage of $V_c = 400\,\text{V}$. The maximum inductance of the inductor is therefore given by $V_c > \max\left(v_{pos} + v_{L,cp} - v_{MN}\right)$ and therefore calculated by

$$L_{c,max} < \frac{1 - \frac{2|v_{off}|}{V_c} - \frac{\sqrt{3}}{2}M}{\frac{\sqrt{3}}{L_{DC}}M\left(1 - \frac{3}{\pi}\right) + \frac{\hat{I}\omega}{2V_c}} \tag{14}$$

where v_{off} is the offset of the midpoint voltage v_{MN} according to the voltage balancing concept (discussed in [13]) and $\hat{I}_N$ the AC-side sinusoidal input current peak value depending on the output load situation. Continuous conduction mode (CCM) to discontinuous conduction mode (DCM) boundary can be found if the ripple of i_{pos} (defined due to the ripple of i_{cp}) reaches zero

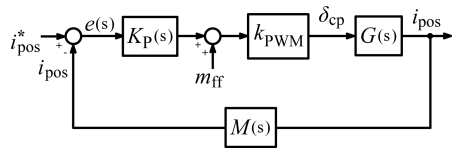

Fig. 12: Closed loop current controller structure valid for continuous conduction mode of the active rectifier system using a FCC.

(as discussed in section II). The minimum allowable inductance value is therefore defined by

$$L_{c,\min} = \frac{M V_c^2 \left(\frac{3}{4}M - \frac{1}{2\sqrt{3}}\right)\left(1 - \frac{\sqrt{3}}{2}M\right)}{f_s P_{o,\min}} \tag{15}$$

for a given minimum output power $P_{o,\min}$ (and defined FCC DC voltages V_c), where the described side effects during light/no-load mode do not occur. Considering a rated output power of 10 kW and a switching frequency of 10 kHz, a current ripple of $\Delta i_{cp} = 20\,\% \cdot \max|i_{cp}(\varphi_N)| = 2.4\,\mathrm{A}$ would lead to a CCM/DCM boundary of 0.68 kW which is 7 % of the rated output power P_o.

V. Current/Voltage Controller Issues

A. Voltage/Balancing Controller

As discussed in [13] the voltage balancing controller (regarding FCC DC voltages v_{cp} and v_{cn}) capability is defined by a linear dependency of v_{off} and P_{in}. Considering an ideal system, the FCC would not be able the guarantee equal DC voltage levels during no-load mode (due to $P_{in} = 0$). The real system, however, includes passive symmetry resistors at the output which advantageously serve as minimal load P_{min} ($i_{L,avg} \neq 0 \rightarrow i_{pos,avg} \neq 0$) during "no-load" at the output of the system $I_o = 0\,\mathrm{A}$. The non ideal active system furthermore includes DC- and AC-resistive components of inductors and equivalent series resistances of capacitors which yield additional losses that have to be compensated by the voltage controller which means further increased input power. The equivalent conductance value g_e^* and hence the input power P_{in} are not equal 0 and therefore the FCC DC voltages can still be controlled and balanced during no- and light-load operation.

B. Current Controller Implementation

As discussed in [10] the current controller can be implemented as simple P-type controller in combination with the modulation feed forward-term

$$m_{ff}(s) = \frac{v_{pos}}{V_c} + \frac{s L_c i_L}{V_c\,(1 + s T_c)} \tag{16}$$

as the system transfer function can be reduced to

$$G(s) = \frac{i_{pos}(s)}{\delta_{cp}(s)} = \frac{V_c}{s L_c}\,. \tag{17}$$

The low-pass filter term $1/(1 + sT_c)$ in the feed forward-term is required to omit amplification of high frequency noise due to the derivative element (D-element) component. Assuming $K_P(s) = k_p$ (simple P-type controller), the closed loop system

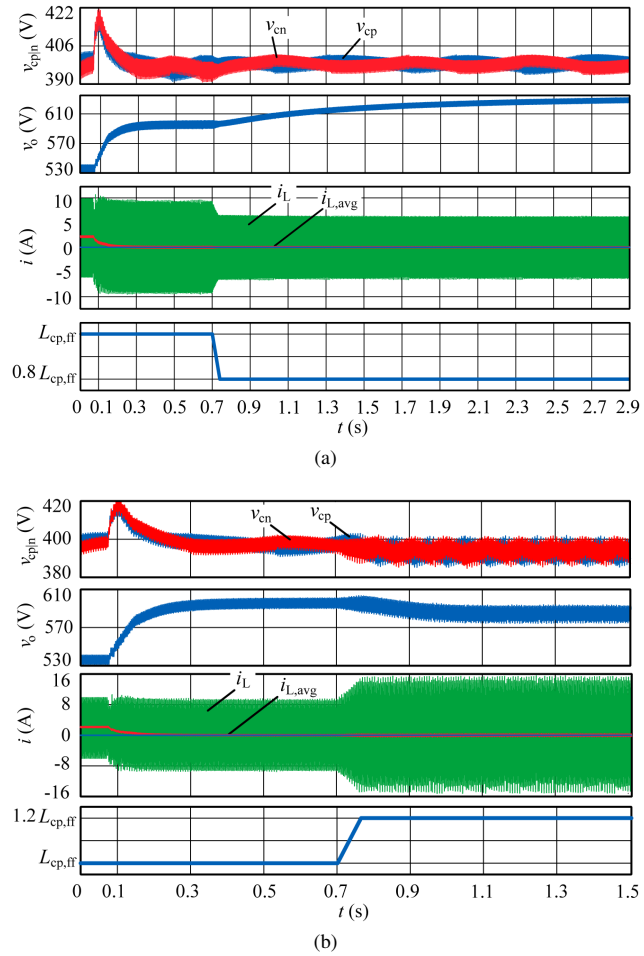

Fig. 13: Loadstep from 1 kW to 0 W. After approximately 0.7 s the feedforward inductance value is going to be (a) decreased (resulting in reduced low-frequent current ripple, losses, extenuated FCC DC voltage balancing capability and raised steady state output voltage V_o) or (b) increased (causing higher low frequency current ripple, losses, improved FCC DC voltage balancing capability and diminished steady state output voltage V_o).

calculates to

$$\frac{i_{pos}}{i^*_{pos}} = \frac{K_P(s)\,G(s)}{1 + K_P(s)\,G(s)} \tag{18}$$

and is depicted in **Fig. 12**, whereas k_{PWM} is of constant value and generally assumed to be 1 , and $M(s)$ is the transfer function of the current transducer which is basically modelled as low-pass filter structure, however, is also neglected and assumed as ideal current transducer ("1") for further calculations. The permanent control deviation $\left(\lim_{s\to 0} s \cdot e(s)\right)$ hence calculates to

$$\lim_{s\to 0} s \cdot e(s) = \lim_{s\to 0} s\,\frac{1}{s}\,\frac{1}{1 + K_P(s)\,G(s)} = 0 \tag{19}$$

A P-type controller would be perfectly applicable, for continuous conduction mode (CCM) and no occuring disturbances of the AC-side mains. During no-load mode, however, the increased output voltage can be observed as disturbance from a point of view of the current controller and basically results in $v_{pos} + \Delta v_{pos}$ instead of v_{pos}. If the AC-side mains voltages

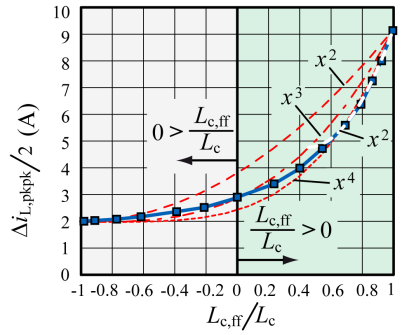

Fig. 14: DC-side smoothing inductance peak current characteristic for modified values of the feedforward to implemented injection inductance ratio $L_{c,ff}/L_c$ for an assumed section of $[-1 \ldots 1]$, valid during no-load operation.

are measured for generation of v_{pos}, no information about Δv_{pos} is available for the FCC system and hence has to be fully compensated by the controller. Δv_{pos} can furthermore be written as $\Delta v_{pos} = V_{o,idle}/2$ for steady state operation. Recalculating the permanent control deviation for disturbed input conditions,

$$\lim_{s\to 0} s \cdot e(s) = \lim_{s\to 0} s \, \frac{\Delta v_{pos}}{V_c} \frac{G(s)}{1 + K_P(s)\, G(s)} = \frac{1}{\omega_c L_c} \neq 0 \quad (20)$$

can be found. The P-type controller is hence not possible to compensate the occuring disturbance and the system cannot be considered to be stable anymore. A PI-type controller ($K_P(s) = k_p + \frac{k_I}{s}$) should therefore replace the P-type controller structure. Considering the adapted conditions the permanent control deviation computes to be

$$\lim_{s\to 0} s \cdot e(s) = \lim_{s\to 0} s \, \frac{1}{s} \, \frac{\frac{1}{sL_c}}{1 - \frac{V_c}{sL_c}\left(k_p + \frac{k_I}{s}\right)} = 0 \, . \quad (21)$$

A PI-type controller is hence mandatory to allow the current control system compensation of occuring distortions evoked due to increased output voltage during no-load mode operation.

C. Optimization Issues

During no-load operation the passive diode bridge is alternately conducting and blocking for defined time instants. During these instants where the diodes are blocking, $i_{cp} = i_L$ and the DC-side smoothing inductance current is hence controlled via the two half-bridge current controllers. The feedforward injection inductance $L_{c,ff}$ can therefore advantageously be used to increase or decrease the 300 Hz peak-to-peak current ripple of i_L by variations of the $L_{c,ff}/L_c$ ratio during light- or no-load operation. A reduced peak-to-peak current ripple, however, results in an increased steady state output voltage $V_{o,idle}$ and reduced FCC DC voltage balancing capability and vice versa. During no-load operation the current controller hence allows a degree of freedom for either reduced no-load operation losses (due to reduced peak-to-peak DC-side choke) shown in **Fig. 13(a)** or reduced steady state output voltage $V_{o,idle}$ and increased balancing capability (depicted in **Fig. 13(b)**). **Fig. 14** depicts the DC-side smoothing choke peak-to-peak current value dependency of the feedforward (fictitious, $L_{c,ff}$) to real injection inductance (L_c) ratio. As can be seen, the characteristic can be approximated by a third or fourth order polynomial. If an interpolation for a specific area is performed (as for example $0.6 < L_{c,ff}/L_c < 1$) an almost immaculate quadratic behaviour can be observed which allows an $ax^2 + b$ approximation (cf., **Fig. 14**, white dashed line) for this sector. Even for infinitely small negative values of the feedforward inductance, the current ripple never appears to be 0 A as it is still partly defined due to the AC-side mains voltages if the passive bridge is conducting. The minimum value of the achievable low-frequency peak-to-peak current is hence dependent on the blocking time instants evoked due to the FCC.

TABLE I: Design Specifications of the Built Three-Phase Rectifier using a FCC.

Mains voltage:	$V_{LL} = 400\,V_{rms}$
Mains frequency:	$f_N = 50\,Hz$
Switching frequency:	$f_s = 10\,kHz$.
FCC dc-link voltage:	$V_{cp} = V_{cn} = 400\,V$
Output power:	$P_o = 10\,kW$

TABLE II: Power Devices Selected for Implementation of the FCC Prototype.

$S_{ia,b}$	1200 V/40 A IGBT, IKW40T120, Infineon
$S_{c\frac{p}{n}\pm}$	600 V/20 A IGBT, IKW20N60H3, Infineon
$D_{h3\pm}$	1200 V/15 A, STTH1512W, ST-Microelectronics
$C_{c\frac{p}{n}}$	470 μF/400 V, EPCOS B43501-type
L_{cp}=L_{cn}=L_{h3}	Iron core 3UI75b, N = 75 turns
	2.5 mH @ 150 Hz, 1.8 mH @ 10 kHz
C_F, C_S	6.8 μF/275 V_{AC}, MKP X2, Arcotronics
C_o	2.2 mF/400 V, Felsic CO 39 A728848
L_{DC}	2.25 mH, Iron core 2 x UI60a
$D_1 - D_6$	35 A/1600 V, 36MT160, Vishay

VI. Experimental Results

Detailed specifications of the implemented 10 kW/10 kHz active rectifier employing a FCC during no-load condition, applied power semiconductor devices and passive components are given in TABLE I and TABLE II. **Fig. 15(a)-(c)** illustrate measurement results considering light- and no-load operation (operating in OM_{II}). For an output power of 2.2 kW (cf., **Fig. 15(a)**) no 10 kHz current ripple considering DC-side smoothing inductor current i_L can be observed. As given in **Fig. 15(c)** no-load operation, however, leads to a superimposed 10 kHz voltage ripple considering v_L and v_{rec} which causes a 10 kHz current ripple of i_L. The 300 Hz DC-side smoothing inductor ripple is still present during no-load mode (circular current). This current causes additional losses in the FCC, the coupled three-phase inductor, the DC-side smoothing inductor and the DC-link (output) capacitor. Hence, measurement results of the active input power yield rather high values of $P_{L,FCC,meas} = 60\,W$ during no-load operation. A conventional passive three-phase rectifier, on contrary, only causes losses due to passive balancing resistors of the electrolytic capacitors during idle mode (as $i_L = i_{pos} = i_{neg} = 0$) and has therefore be measured with only $P_{L,B6,meas} = 8\,W$ which is $\approx 13\,\%$ regarding the losses of the active system.

As can be seen from **Fig. 15(b)**, even for light-load operation v_{rec} and v_L are stressed with high frequency voltage components

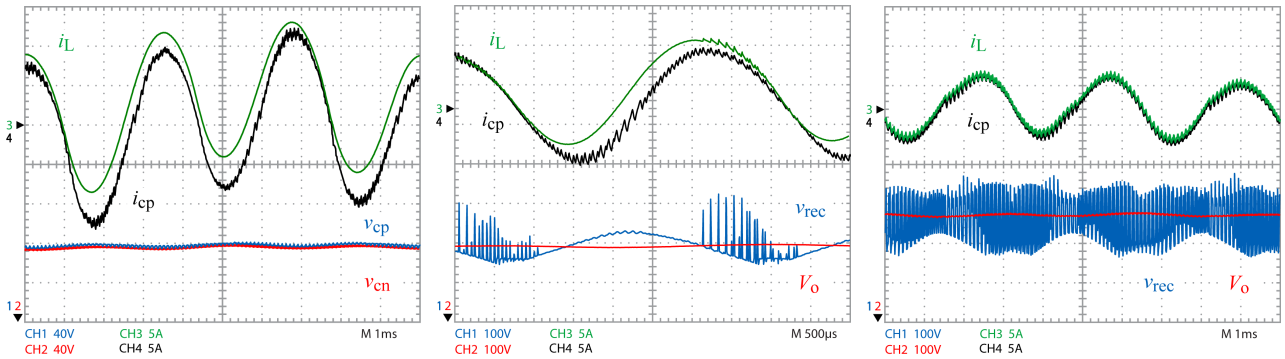

(a) (b) (c)

Fig. 15: Measurement results of the active system during CCM, ICOM and no-load mode operating in $\mathrm{OM_{II}}$. (a) Injection and smoothing inductance current (i_{cp}, i_{L}) and FCC DC voltages for 1.33 kW output power. No high-frequency components can be observed regarding i_{L} during CCM. (b) 0.8 kW output power (ICOM) for an injection inductance value of $< 1.8\,\mathrm{mH}$ @ 10 kHz. The rectifier output voltage v_{rec} and hence v_{L} shows high frequency voltage ripple with switching frequency during those time instants where i_{pos} yields discontinuous behaviour. (c) No-load operation and according side effects of the active system (circulating inductance current with high frequency current ripple), however, shows reduced 300 Hz peak-to-peak current ripple due to downscaled feed forward value ($L_{\mathrm{c,ff}}/L_{\mathrm{c}} \approx 0.64$).

during those time instants where i_{pos} shows intermittent sections. Comparing **Fig. 15(a)** and **Fig. 15(c)** a different $\Delta i_{\mathrm{L,pkpk}}$ and an increased output voltage V_{o} is observable. During continuous conduction mode (CCM) the peak-to-peak current ripple is defined due to the DC-side smoothing inductance and therefore yields $\approx 18\,\mathrm{A}$. For no-load operation ($\mathrm{OM_{II}}$) $\Delta i_{\mathrm{L,pkpk}}/2$ decreased to $\approx 6\,\mathrm{A}$ which results due to optimized loss operation (and hence downscaled feed forward value $L_{\mathrm{c,ff}}/L_{\mathrm{c}} \approx 0.64$, cf., **Fig. 14**) as discussed in section V.*C*.

VII. Conclusion

In this paper no- and light-load conditions of an active three-phase rectifier based on the third harmonic injection principle employing a FCC are discussed in detail. Numerous effects occuring during both conditions (increased steady state output voltage V_{o}, common-mode voltage ripple with switching frequency, current stress of DC-side smoothing inductance with switching frequency, distorted midpoint voltage v_{MN} and control issues,) are addressed and analyzed. Operating mode boundaries of passive and active topologies are furthermore specified. Three-different operating modes during no-load mode are listed ($\mathrm{OM_I}$ - FCC activated and bidirectional switches deactivated, $\mathrm{OM_{II}}$ - system fully operating, $\mathrm{OM_{III}}$ - FCC and bidirectional switches deactivated) and examined in detail. Considering continuous to discontinuous boundary, design guidlines for the three-phase inductance L_{c} are enhanced which is primarily affecting this threshold. Proper operation of current and voltage controllers is finally verfied and optimization alternatives (regarding losses, output voltage value and balancing capability) are addressed. Experimental results of an implemented 10 kW/10 kHz active rectifier operating in $\mathrm{OM_{II}}$ ultimately provides promising results of the active system for these load conditions.

Acknowledgment

The authors are very much indebted to the Austrian Research Promotion Agency (FFG) which generously supports the work of the Vienna University of Technology Power Electronics Section (Institute of Energy Systems and Electrical Drives).

References

[1] J.W. Kolar and T. Friedli, "The Essence of Three-Phase PFC Rectifier Systems—Part I," *IEEE Transactions on Power Electronics*, vol. 28, no. 1, pp. 176–198, 2013.

[2] T. Friedli, M. Hartmann, and J.W. Kolar, "The Essence of Three-Phase PFC Rectifier Systems—Part II," *IEEE Trans. on Pow. Electron.*, vol. 29, no. 2, pp. 543–560, 2014.

[3] J.W. Kolar and F.C Zach, "A Novel Three-Phase Three-Switch Three-Level Pwm Rectifier," in *Proceedings of the Conference for Power Electronics, Intelligent Motion, Power Quality (PCIM)*, Nuernberg, Germany, June 28-30 1994, pp. 125–138.

[4] T.B. Soeiro, T. Friedli, and J.W. Kolar, "Swiss rectifier — A Novel Three-Phase Buck-Type PFC Topology for Electric Vehicle Battery Charging," in *Proceedings of the Twenty-Seventh Annual IEEE Applied Power Electronics Conference and Exposition (APEC)*, 2012, pp. 2617–2624.

[5] H. Yoo and Seung-Ki Sul, "A New Circuit Design and Control to Reduce Input Harmonic Current for a Three-Phase AC Machine Drive System having a very Small DC-link Capacitor," in *Proceedings of the Twenty-Fifth Annual IEEE Applied Power Electronics Conference and Exposition (APEC)*, 2010, pp. 611–618.

[6] IEEE Std 519-1992, *IEEE Recommended Practices and Requirements for Harmonic Control in Electrical Power Systems*, New York, NY: IEEE, 1992.

[7] EC61000-3-2, *Electromagnetic compatibility (EMC) Part 3-2: Limits for harmonic current emissions (equipment up to and including 16 A per phase)*, published by the International Electrotechnical Commission (IEC), 2000.

[8] J.W. Kolar and H. Ertl, "Status of the Techniques of Three-Phase Rectifier Systems with Low Effects on the Mains," in *Proceedings of the Twenty-First InternationalTelecommunication Energy Conference (INTELEC)*, 1999.

[9] M. Hartmann and R. Fehringer, "Active Three-Phase Rectifier System Using a "Flying" Converter Cell," in *Proceedings of Energy Conference and Exhibition (ENERGYCON), 2012 IEEE International*, 2012, pp. 82–89.

[10] M. Hartmann, R. Fehringer, M. Makoschitz, and H. Ertl, "Design and Experimental Verification of a Third Harmonic Injection Rectifier Circuit Using a Flying Converter Cell," in *Proceedings of the Twenty-Ninth Annual IEEE Applied Power Electronics Conference and Exposition (APEC)*, 2014, pp. 920–927.

[11] J. Schaefer, *Rectifier Circuits - Theory and Design*, John Wiley & Sons, INC., New York, 1965.

[12] M. Leibl, Johann. W. Kolar, and J. Deuringer, "New Current Control Scheme for the Vienna Rectifier in Discontinuous Conduction Mode," in *Proceedings of the Energy Conversion Congress and Exposition (ECCE)*, Pittsburgh, USA, Sept. 14-18 2014, pp. 1240–1247.

[13] M. Makoschitz, M. Hartmann, H. Ertl, and R. Fehringer, "DC Voltage Balancing of Flying Converter Cell," in *Proceedings of the Energy Conversion Congress and Exposition (ECCE)*, Pittsburgh, USA, Sept. 14-18 2014, pp. 4071–4078.